



Contents lists available at ScienceDirect

Arabian Journal of Chemistry

journal homepage: www.ksu.edu.sa

Pd octahedra nanocubes mediated photo-fenton catalytic performance for sustainable degradation of methylene blue

Heying Li^{a,1}, Ding Luo^{b,1}, Pengshan Guo^a, Shegan Gao^{a,*}, Manping Lin^b, Hongbo Sun^c, Jianping Wang^c, Dongmei Yu^c, Shaowen Cheng^{b,**}, Jinghua Li^{a,b,c,*}

^a The 1st Affiliated Hospital, College of Medical Technology and Engineering, Henan University of Science and Technology, Luoyang 471000, China

^b Key Laboratory of Hainan Trauma and Disaster Rescue, Department of Wound Repair, the First Affiliated Hospital of Hainan Medical University, School of Emergency and Trauma, Hainan Medical University, Haikou 570100, China

^c Key Laboratory of Hainan Trauma and Disaster Rescue, The First Affiliated Hospital of Hainan Medical University, College of Emergency and Trauma, Hainan Medical University, Haikou 5711'99, China

ARTICLE INFO

Keywords:

Pd octahedra
Tip-shaped structure
Photothermal conversion
Fenton reaction
Methylene blue
Degradation

ABSTRACT

This research utilized a typical solvothermal approach, by employing Na_2PdCl_4 as the synthetic precursor, L-ascorbic acid (AA) as the reductant agent, and polyvinylpyrrolidone (PVP) as the practical surfactant, palladium (Pd) octahedra was finally effectively synthesized by the hydrothermal and solvothermal methods. Subsequently, characterizations of Pd octahedra were conducted by using TEM, XPS, XRD, and other analytical methods. Whereafter, Pd octahedra displayed a consistent shape and size, featuring a distinctive tip-shaped structure, which conferred upon them outstanding optical absorption properties within the near-infrared (NIR) region. Consequently, under NIR laser exposure, Pd octahedra could elevate local reaction temperature via in-situ photothermal conversion, thereby stimulating the formation of active sites of Fenton catalysts. The Photo-Fenton catalytic activity of Pd octahedra was investigated by using methylene blue (MB) as a model pollutant. The degradation efficiency of MB reached 94.8 % within 35 min under 808 nm laser irradiation, and the removal rate of MB by Pd octahedra could still reach more than 90 % after five cycles of use. All the results manifest that Pd octahedra exhibit excellent purification performance for MB dyestuff wastewater.

1. Introduction

The escalating challenges of global water pollution, driven by economic globalization and population growth, have spurred widespread demand for clean water sources worldwide (Tian et al., 2024; Lushaj et al., 2024; Yu et al., 2024; Zhang et al., 2024). Effective treatment and regeneration of organic wastewater is a crucial strategy for addressing water scarcity and ensuring clean water provision. Advanced Oxidation Processes (AOPs) could highly output reactive oxygen species substance (ROS), such as hydrogen peroxide (H_2O_2), hydroxyl radicals ($\bullet\text{OH}$), sulfate radicals ($\text{SO}_4\bullet$), singlet oxygen ($^1\text{O}_2$), and superoxide anion radicals ($\bullet\text{O}_2^-$), which directly mineralize organic pollutants or enhance their biodegradability. AOPs are characterized by their potent oxidation

capacity, high treatment efficiency, and operational simplicity, promising significant advancements in sustainable water restoration and purification (Liu et al., 2024; Bi et al., 2024; Lu and Liu, 2024; Yan et al., 2024; Tian et al., 2024).

Among the array of AOPs, the Fenton reaction, facilitated by Fe^{2+} to yield $\bullet\text{OH}$ from H_2O_2 , emerges as an eco-friendly, efficient, and energy-conserving advanced oxidation process has been extensively utilized in water pollution management (Yu et al., 2024; Liu et al., 2024). Nonetheless, conventional Fenton setups confront multiple limitations, including a restricted pH spectrum, catalyst non-recoverability, generation of substantial iron sludge, and sluggish iron cycling kinetics. To address these challenges, scholars have shifted their focus towards crafting Fenton-like catalytic systems. These reactions leverage non-iron

* Corresponding authors at: The 1st Affiliated Hospital, College of Medical Technology and Engineering, Henan University of Science and Technology, Luoyang 471000, China.

** Corresponding authors at: Key Laboratory of Hainan Trauma and Disaster Rescue, Department of Wound Repair, the First Affiliated Hospital of Hainan Medical University, School of Emergency and Trauma, Hainan Medical University, Haikou 570100, China.

E-mail address: anubiss1860@163.com (J. Li).

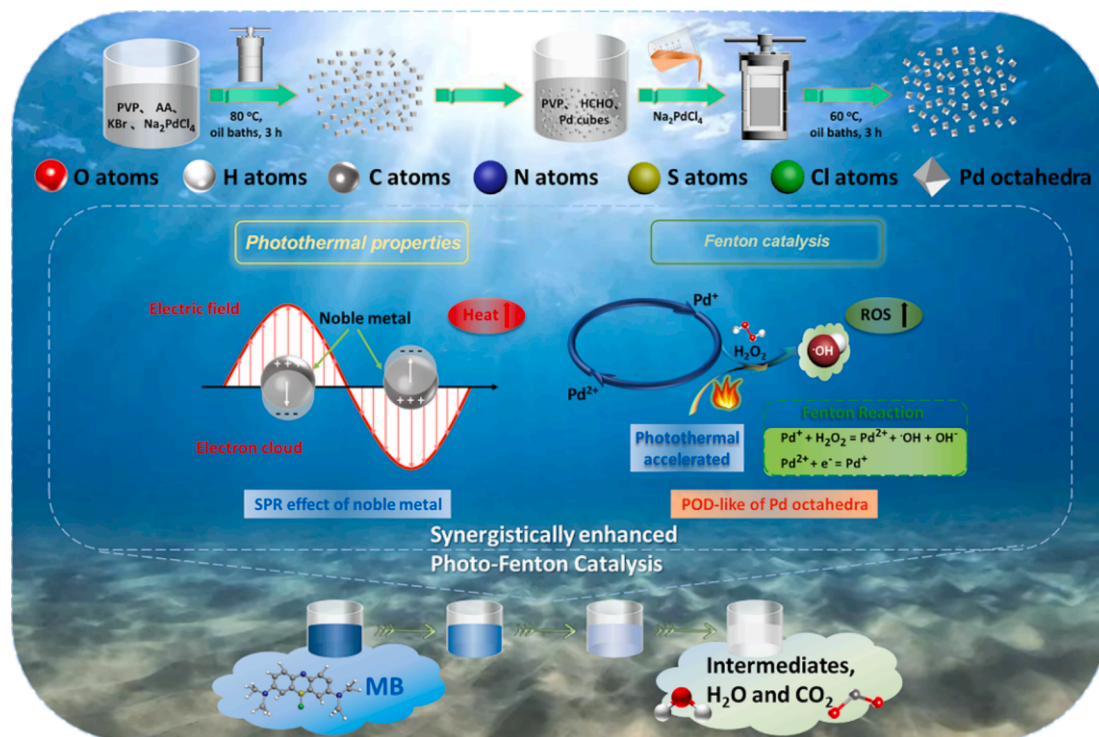
¹ These authors contributed equally to this work.

<https://doi.org/10.1016/j.arabjc.2024.105936>

Received 22 March 2024; Accepted 23 July 2024

Available online 24 July 2024

1878-5352/© 2024 The Authors. Published by Elsevier B.V. on behalf of King Saud University. This is an open access article under the CC BY-NC-ND license (<http://creativecommons.org/licenses/by-nc-nd/4.0/>).



Scheme 1. Synthesis process for Pd octahedra and schematic depiction of its mechanism for degrading MB in wastewater.

transition metal-based catalysts that, upon interaction with H_2O_2 , engender $\bullet\text{OH}$ for degrading organic pollutants (Lian et al., 2024; Zhang et al., 2023; Wu et al., 2023; Jana and Zhao, 2022). Unlike traditional Fenton reactions, these Fenton-like catalytic systems exhibit operability under neutral or even alkaline conditions, thereby broadening their suitability across a diverse range of water matrices (Yan et al., 2021).

Too often, heat frequently plays a pivotal role in influencing chemical reactions. The in-situ photothermal conversion of near-infrared (NIR) photothermal Fenton catalysts facilitates localized heating of catalytic sites, thereby boosting catalytic activity and enhancing the degradation efficiency of organic pollutants (Zhu Y., Zhao R., Feng L., Wang W., Xie Y., Ding H., Liu B., Dong S., Yang P., Lin J., Defect-Engineered Tin Disulfide Nanocarriers as “Precision-Guided Projectile” for Intensive Synergistic Therapy, *Small Methods*, 2024; Zhao et al., 2024; Wang et al., 2023; Li et al., 2022). However, research on NIR triggered photothermal Fenton catalysts is still in its developmental phase, mainly concentrating on semiconductor and carbon materials with broad spectrum absorption (Zhang et al., 2023; He et al., 2018; Gao et al., 2023). To broaden the range of catalyst types and extend the application scope of NIR photothermal Fenton catalysis, exploring alternative NIR photothermal Fenton catalytic materials holds significant importance.

Plasma effect has shown remarkable performance in photothermal catalysis, leading to the synthesis of various plasma nanoparticles. Gold and silver nanoparticles are commonly utilized, particularly nanospheres and nanorods, which are highly favored in the field of nanoplasmonics (Yang et al., 2024; Schuknecht et al., 2023; Liao et al., 2024; Sibug-Torres et al., 2024; Awiaz et al., 2023). For example, gold nanorods display robust longitudinal plasmon absorption bands within the NIR spectrum and exhibit efficient photothermal conversion when stimulated by NIR light, making them valuable for NIR photothermal catalysis studies (Skillin et al., 2024; Zhang et al., 2023; Seo et al., 2014; Zhao et al., 2022). However, chemically synthesized gold nanorods often lack uniform shapes and sizes, resulting in broad plasma peaks and limited local electric field enhancement due to rounded or flattened ends. Consequently, researchers have tailored the longitudinal plasma

wavelengths by synthesizing gold nanobipyramids with sharp tips. Compared to gold nanorods, gold nanobipyramids offer enhanced the local strength of electric field, larger optical cross sections, thereby boosting their photothermal conversion efficiency and optimizing the utilization of NIR light (Chow et al., 2019; Kesharwani et al., 2023; Zhang et al., 2023; Palani et al., 2023; Yang et al., 2024; Meng et al., 2024; Kim et al., 2024; Ali et al., 2023).

Drawing inspiration from this, our project utilized palladium (Pd) cubes as the starting material, modifying their ends to synthesize Pd octahedra successfully. With two sharp tips, Pd octahedra exhibit enhanced local electric field effects and magnify the Local electron density of photon at the nanoscale, thereby enhancing the efficiency of converting NIR light. By combining catalytic and photothermal centers, Pd octahedra demonstrates photothermal and Fenton catalytic properties, facilitating the efficient oxidation of dye organic pollutants in wastewater, such as methylene blue (MB) molecules (Scheme 1). This investigation delves into the NIR photothermal conversion efficiency and Fenton catalytic activity of Pd-based plasma, further extending their utility in treating dye wastewater.

2. Experimental methods

2.1. Chemicals and reagents

Sodium tetrachloropalladate (Na_2PdCl_4 , 98 %), polyvinylpyrrolidone (PVP, $\text{MW} \approx 56,000$), methylene blue (MB, ≥ 98.5 %), hydrogen peroxide (H_2O_2 , 30 %) and formaldehyde solution (CH_2O) were bought from Aladdin (Shanghai, China). L-ascorbic acid (AA, 99.99 %) and 3,3',5,5'-tetramethylbenzidine (TMB, ≥ 99.99 %) were obtained from Macklin Reagent Company (Shanghai, China). All drugs and chemical reagents were utilized immediately upon opening, requiring no additional processing. Deionized water was exclusively employed in preparing all experimental solutions.

2.2. Preparation of Pd octahedra

Pd nanocubes were synthesized directly by the solvothermal methods (Zhang et al., 2015). First, 630.0 mg of PVP, 360.0 mg of AA, and 3600.0 mg of KBr were dissolved in 48.0 mL of water, and then added the configured solution of Na_2PdCl_4 (18.0 mL, 19.0 mg mL^{-1}). After that, the mixed solution was heated under 80 °C oil bath for 3 h to obtain Pd nanocubes.

Subsequently, these Pd nanocubes (1.8 mg mL^{-1}) were immersed in a formaldehyde solution containing PVP and heated in a oil bath (90 °C) for 15 min to ensure the complete dissolution of PVP. Then, added Na_2PdCl_4 (2.0 mL, 15.0 mg mL^{-1}) into the preheated solution and finally the mixed solution was heated under 60 °C oil bath for 3 h. After centrifugation and washing steps, the obtained product was termed Pd octahedra and dried overnight in vacuum oven.

2.3. Instruments

Transmission electron microscopy (TEM, JEOL JEM-2100, Japan) and energy dispersive X-ray spectroscopy (EDS) were utilized to examine the morphological features and surface element distribution of Pd octahedra catalysts. X-ray diffraction (XRD, Bruker D8-Advance, Germany) was measured to analyze the crystalline properties and crystal face information of Pd octahedra. X-ray photoelectron spectroscopy (XPS, ULVAC PHI X-tool, Japan) was applied for fitting the orbital states and elemental valence states of Pd octahedra. UV-visible spectrophotometer (NanoDrop-1, Thermo Scientific, America) was used to measure the absorption spectra of Pd octahedra in the NIR region, with changes in characteristic absorption peaks of TMB and MB indicating TMB oxidation and MB decomposition. Electron paramagnetic resonance (EPR, Bruker EMXnano, Germany) was employed to further resolve the type of ROS generated in the Fenton reaction and calculate the energy of $\bullet\text{OH}$ in different catalytic groups.

2.4. Photothermal experiment

To assess the thermal response behavior of the material under illumination, we employed an 808 nm NIR laser to irradiate a solution of Pd octahedra. A handheld infrared thermometer was used to record the temperature rise and infrared thermal graphic images of Pd octahedra under different concentrations. To investigate the photothermal stability of the catalyst, five consecutive cycles of experiments were conducted (5 min of laser irradiation followed by 5 min of shutdown), comparing the temperature variation for each cycle. Real-time recording of the cooling rate of the photothermal system in the external environment was carried out to calculate its cooling time constant (τ_s), the calculation formula is based on Ren's report (1) (Ren et al., 2015):

$$\tau_s = \frac{t}{-\ln\theta} \quad \theta = \frac{T_{\text{surr}} - T}{T_{\text{surr}} - T_{\text{max}}} \quad (1)$$

In this context, t represents the cooling duration, T signifies the temperature after t of cooling, T_{surr} denotes room temperature, and T_{max} stands for the highest stable temperature.

2.5. Fenton catalytic activity

In this study, TMB was used as a model dye to detect the products of the $\bullet\text{OH}$ in the Fenton reaction between Pd octahedra and H_2O_2 . The catalyst and H_2O_2 were added to a hydrochloric acid buffer solution (pH 5.0) containing TMB, and the mixture was allowed to react sufficiently under appropriate temperature and time conditions. The absorbance of the reactive solution was measured by using the spectrophotometer, and any color changes were recorded. By varying the concentration of H_2O_2 added, the kinetic behavior of the Fenton catalytic reaction involving Pd octahedra was investigated. According to the Lambert-Beer law

($A = \epsilon \cdot c \cdot l$, where A is the absorbance of the solution, ϵ is the molar absorptivity with $\epsilon = 39000 \text{ M}^{-1} \text{ cm}^{-1}$, c is the molar concentration of the solute, and l is the path length with $l = 10 \text{ mm}$), the concentration of TMB was determined and its rate of concentration change was calculated. A scatter plot was created using Origin software with H_2O_2 concentration as the x-axis and the rate of change of TMB concentration as the y-axis, and fitted using the Michaelis-Menten equation (2) (Chen et al., 2021).

$$y = \frac{V_{\text{max}} \cdot x}{K_M + x} \quad (2)$$

In this equation, y represents the substrate conversion rate, V_{max} represents the maximum reaction rate, x represents the substrate concentration, and K_M represents the Michaelis constant.

By appropriately rearranging Eq. (2), denoted as Eq. (3) (Chen et al., 2021), and using the reciprocal of H_2O_2 concentration and the reciprocal of the rate of TMB concentration change as the x-axis and y-axis, respectively, the Lineweaver-Burk plot can be fitted. This approach provides a more intuitive demonstration of the catalytic activity of Pd octahedra as peroxidase-like enzyme participating in the Fenton reaction.

$$\frac{1}{y} = \frac{K_M}{V_{\text{max}}} \cdot \frac{1}{x} + \frac{1}{V_{\text{max}}} \quad (3)$$

2.6. Degradation experiments of MB

The study investigated the efficiency of Fenton degradation of wastewater containing MB under different water bath temperatures and NIR light irradiation. Pd octahedra ($125.0 \mu\text{g mL}^{-1}$) were placed in simulated wastewater containing MB (50.0 mg/L), and the Fenton degradation process was initiated by adding H_2O_2 (3 %). The mixed solution was placed in water bath pots at different temperatures (30 °C, 40 °C, 50 °C), with the laser group continuously irradiated using an 808 nm NIR laser (5 min, 1.6 W). Factors such as solution pH, concentration of dye and concentration of catalyst were explored for their influence on the Fenton catalytic reaction to optimize the experimental setup and determine the optimal reaction conditions for achieving the highest efficiency of MB degradation. The solution pH was adjusted using HCl and NaOH, with pH values fixed at 3, 5, 7, 9, and 11. All degradation experiments involved sampling at regular intervals, and changes in absorbance of the mixed solution were recorded using a spectrophotometer. Every experimental group was repeated for 3 times, and the average value was ultimately ensured as the final result, with error bars in the graph representing the range of error. The degradation efficiency of MB was calculated using Eq. (4).

$$\text{Degradation efficiency (\%)} = \frac{(C_0 - C_t)}{C_0} \times 100\% \quad (4)$$

The variables C_0 and C_t in the equation represent the concentration of MB before and after degradation, respectively.

To delve deeper into the temperature's impact on MB degradation rate, pseudo-first-order kinetics analysis was utilized to evaluate catalytic reaction efficiency across various water bath temperature groups. By fitting experimental data to Eq. (5), the rate constant k_1 can be determined.

$$\frac{C_t}{C_0} = \exp(-k_1 \cdot t) \quad (5)$$

The variable t represents the time during the degradation reaction. C_0 and C_t in Eq. (5) has the same meaning as in Eq. (4).

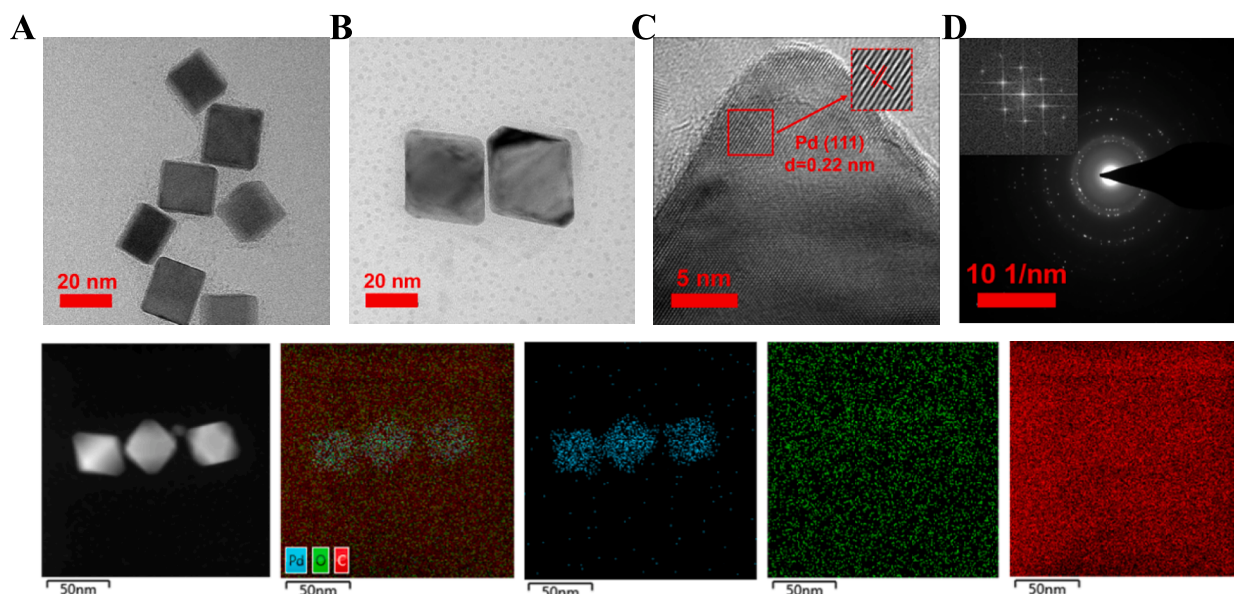


Fig. 1. TEM images of (A) Pd cubes and (B) Pd octahedra. (C) HRTEM image of Pd octahedra. (D) The SAED pattern of Pd octahedra (Left: FFT transformation diagram). (E) Element mapping images of Pd, O, and C of Pd octahedra catalyst.

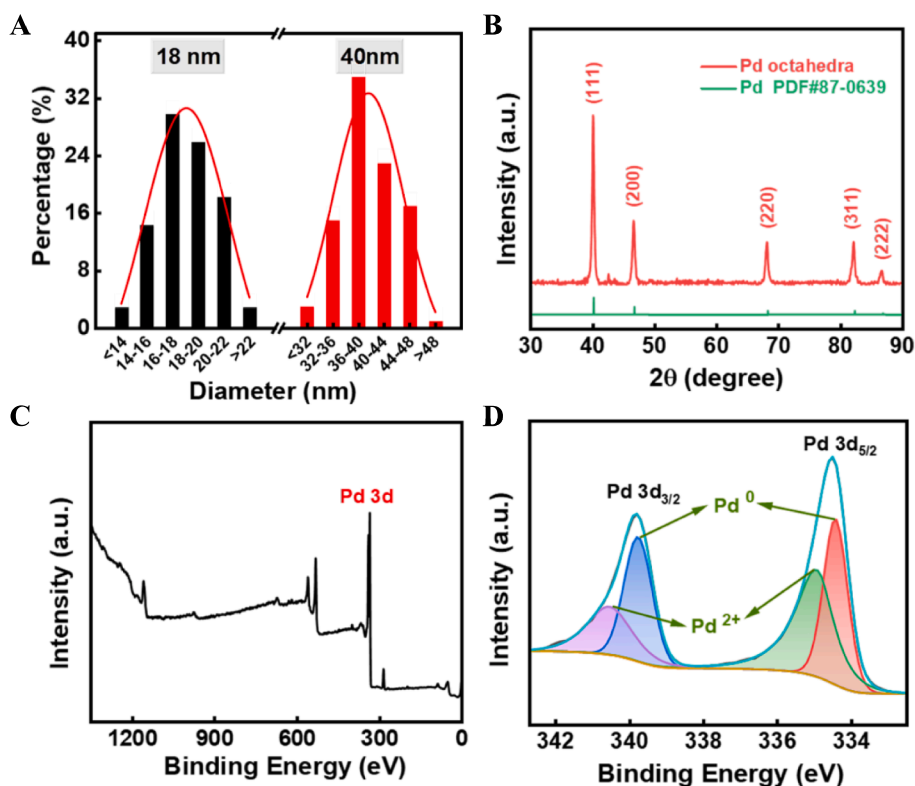


Fig. 2. (A) Particle size distribution of Pd octahedra. (B) XRD pattern of Pd octahedra. XPS spectra of (C) Pd octahedra and (D) Pd 3d.

3. Results and discussion

3.1. Morphology and other characterizations

In the preparation of nanocrystalline catalysts, certain substances are typically required to guide the stacking behavior of atoms on the crystal nucleus, which are called capping agents, and different capping agents often yield different growth outcomes. For instance, by employing KBr as the capping agent, Na_2PdCl_4 as the synthetic precursor, AA as the

reductant agent, and PVP as the practical surfactant, we successfully synthesized Pd nanocubes with uniform morphology and average size of 18 nm (Fig. 1A and Fig. 2A).

However, Pd octahedra are synthesized by using the secondary growth technique, employing PVP as the capping agent, based on the growth of crystal species such as Pd cubes. That is, under the reduction of a weakly reducing formaldehyde solution, Pd atoms generated from the reduction of Na_2PdCl_4 slowly accumulate to the active sites of Pd cubes, gradually forming Pd octahedra (Fig. 1B). The size of the formed

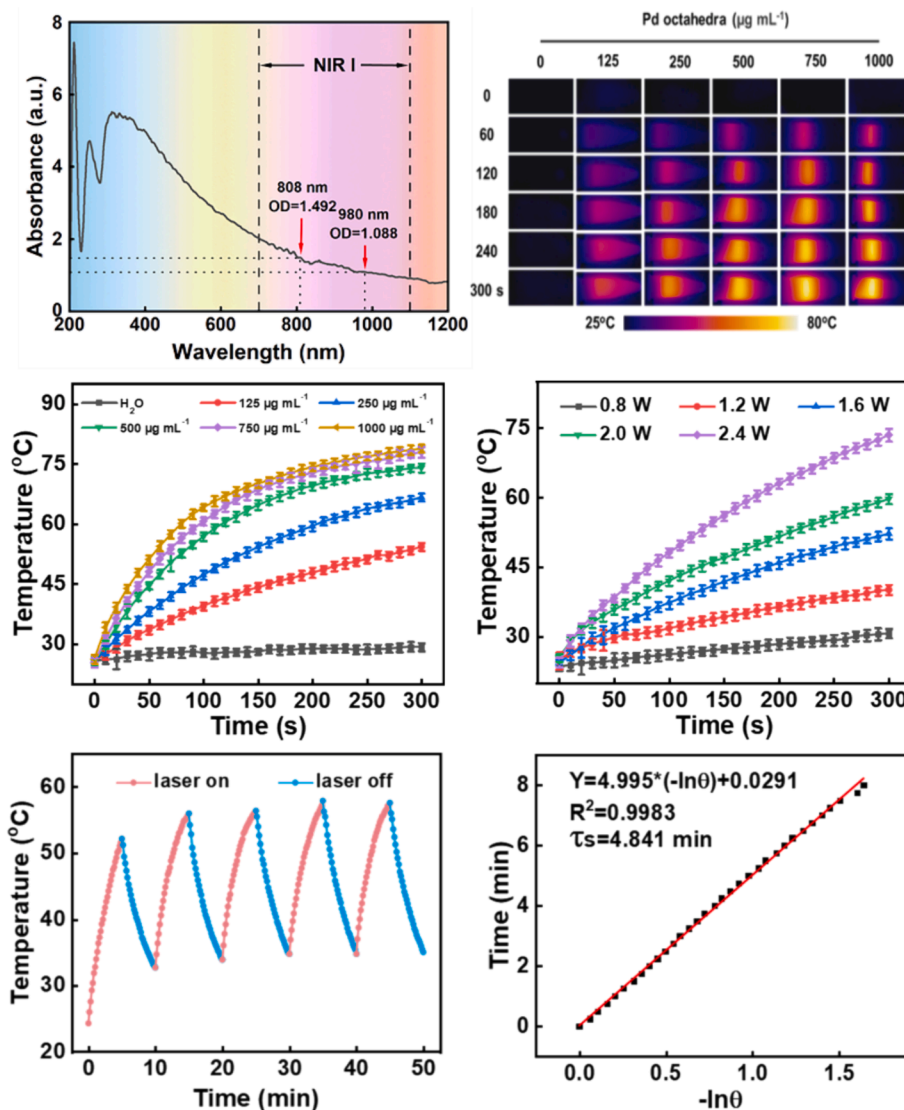


Fig. 3. (A) UV-Vis absorption spectrum of Pd octahedra in the NIR region. (B) Infrared thermal imaging images and (C) heating curves of Pd octahedra at various concentrations under 808 nm NIR light (1.6 W cm^{-2} , 5 min). (D) Temperature elevation curves of Pd octahedra ($125.0 \mu\text{g mL}^{-1}$) by irradiated by 808 nm laser with different power levels. (E) Temperature elevation-decline curves of Pd octahedra over five cycles. (F) The fitting curve of the cooling process of Pd octahedra.

Pd octahedra is 40 nm (Fig. 2A), and with a distance of 0.22 nm between adjacent (111) lattice planes (Fig. 1C). Both selected area electron diffraction pattern (SAED, Fig. 1D) and FFT transformation diagram indicated that the Pd octahedra are single crystals. EDS results (Fig. 1E) showed uniform distribution of Pd signals on their surface, which consistent with the analysis results of XPS (Fig. 2C).

XRD revealed that the positions of the (111), (200), (220), (311), and (222) crystal planes of Pd octahedra and their corresponding diffraction angles were consistent with Pd (PDF#87-0639) (Fig. 2B). Peak fitting of the 3d orbitals of Pd octahedra showed the coexistence of Pd⁰ and Pd²⁺ (Fig. 2D). This multivalent property enables Pd octahedra to undergo transformation between different oxidation states in the Fenton reaction, providing necessary conditions for the Fenton catalytic activity of Pd octahedra, and aiding in the understanding of the mechanism of Pd octahedra catalysts in the Fenton reaction.

3.2. Photothermal performance

Measurements of the absorption characteristics of Pd octahedra under different wavelengths of laser were conducted using a UV-vis spectrophotometer. As illustrated in Fig. 3A, strong and broad

absorption bands were observed in the NIR-I, indicating excellent light absorption property and photothermal conversion capability of Pd octahedra. Subsequently, we investigated the effects of concentration of Pd octahedra and power of laser on the photothermal conversion performance by using an 808 nm NIR laser. As shown in Fig. 3B-D, the temperature rise performance of Pd octahedra was positively correlated with the catalyst concentration and irradiated power of laser. Pd octahedra at a concentration of $125.0 \mu\text{g mL}^{-1}$ exhibited rapid temperature elevation to around $50 \text{ }^\circ\text{C}$ within 5 min by using 1.6 W cm^{-2} laser irradiation, demonstrating its outstanding photothermal conversion capability.

Furthermore, during five cycles of laser on-off irradiation (1.6 W cm^{-2}) experiments, the heating ability of Pd octahedra ($125.0 \mu\text{g mL}^{-1}$) remained essentially unchanged, indicating excellent photothermal stability and the capability to withstand prolonged laser irradiation while maintaining stable heat generation (Fig. 3E). Finally, heating and cooling curves of the Pd octahedra photothermal agent were plotted, and τ_c of 4.841 min was calculated (Fig. 3F), indicating excellent thermal conductivity and thermal response capability of the photothermal system.

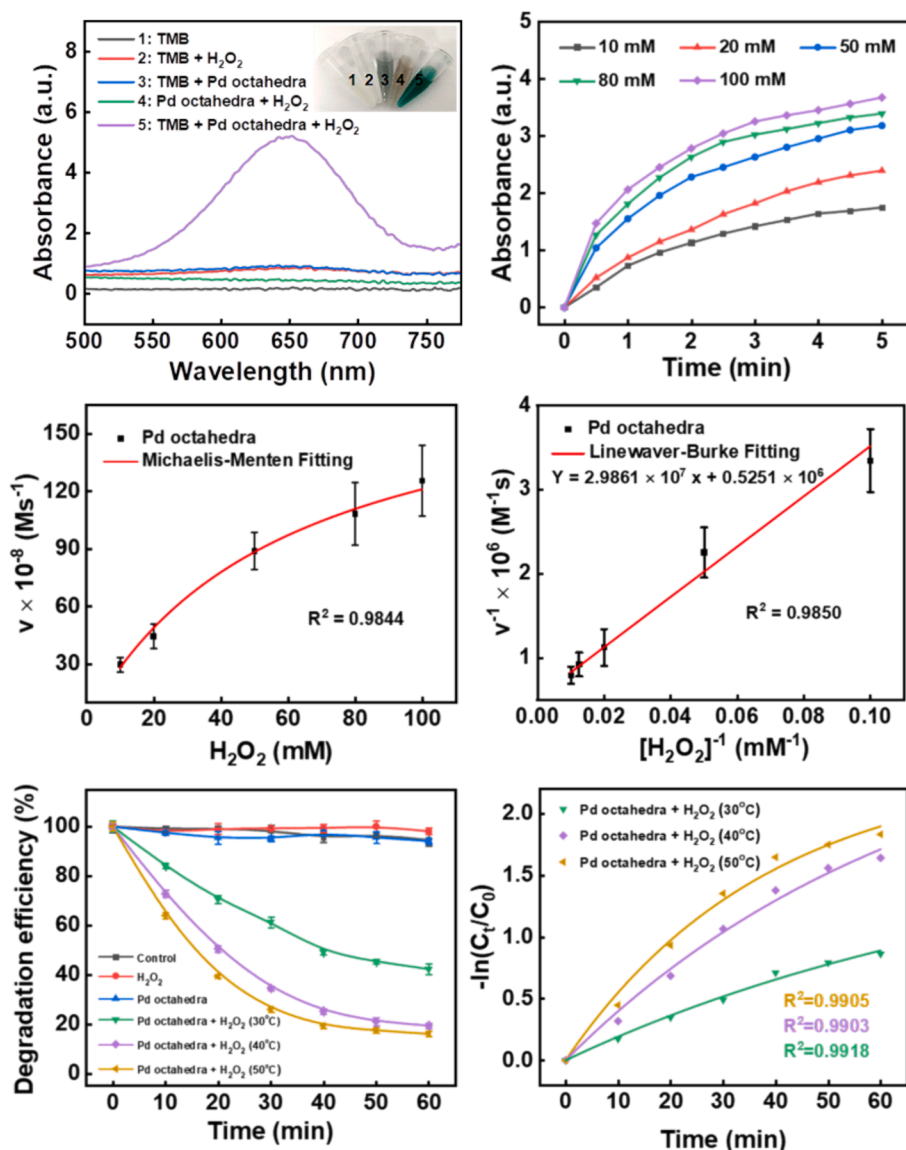


Fig. 4. (A) UV-Vis absorptive spectra depicting the oxidation of TMB by Pd octahedra with H₂O₂ (Concentration of Pd octahedra: 50.0 $\mu\text{g mL}^{-1}$, H₂O₂: 10 mM, TMB: 1 mM). (B) Changes in absorbance values of TMB at 652 nm under treatment with Pd octahedra and different concentrations of H₂O₂. (C) Relative Michaelis-Menten fitting and (D) Lineweaver-Burk fitting. (E) Degradation of MB at various water bath temperatures (Concentration of Pd octahedra: 125.0 $\mu\text{g mL}^{-1}$, H₂O₂: 3 %, MB: 50 mg/L) and (F) the associated catalytic kinetic analysis.

3.3. Detection of •OH

TMB was utilized to evaluate the Fenton catalytic and degradation activity of Pd octahedra. In Fig. 4A, the presence of both Pd octahedra and H₂O₂ led to the oxidation of TMB, resulting in the formation of a blue product and an increase in absorbance at 652 nm, confirming the generation of •OH. Various molar concentrations of H₂O₂ were employed to participate in the Fenton catalytic reaction to examine the catalytic kinetic behavior of Pd octahedra. As depicted in Fig. 4B, with the increase of H₂O₂ concentration, the absorbance at 652 nm exhibited a more pronounced escalation, suggesting an accelerated •OH generation rate.

A scatter plot correlating H₂O₂ concentration with the rate of change in TMB concentration was constructed (Fig. 4C and 4D). This data was fitted using the Michaelis-Menten equation and the Lineweaver-Burk plot, yielding K_m and V_{max} values of 56.855 mM and $1.904 \times 10^{-6} \text{ Ms}^{-1}$, respectively. These findings indicated that Pd octahedra demonstrate a catalytic activity akin to POD enzymes, showcasing robust H₂O₂ binding capability and high efficacy in Fenton catalytic reaction.

3.4. Photothermal-enhanced Fenton catalytic activity

Studies have shown that appropriately increasing the temperature of the Fenton catalytic system can enhance the reaction rate. However, employing heating systems escalates energy consumption and operational expenses in water treatment endeavors. Hence, opting for Fenton catalysts endowed with photothermal properties presents considerable potential for the wastewater treatment sector.

Based on these findings, we investigated the synergistic effect of the photothermal conversion efficiency and Fenton catalysis for dye degradation by using Pd octahedra. Initially, we examined MB degradation under various reaction systems. Fig. 4E illustrates that neither the catalyst alone nor H₂O₂ alone could initiate MB decomposition. Only when Pd octahedra and H₂O₂ were present concurrently, can the Fenton-like reaction be induced to effectively remove MB. Subsequently, we subjected the reaction system to 30, 40, and 50 °C to investigate the acceleration effect of temperature on MB degradation rate. UV-vis absorption spectra and optical images of solutions at different time points are depicted in Fig. 5A-D. The outcomes demonstrate that the system at

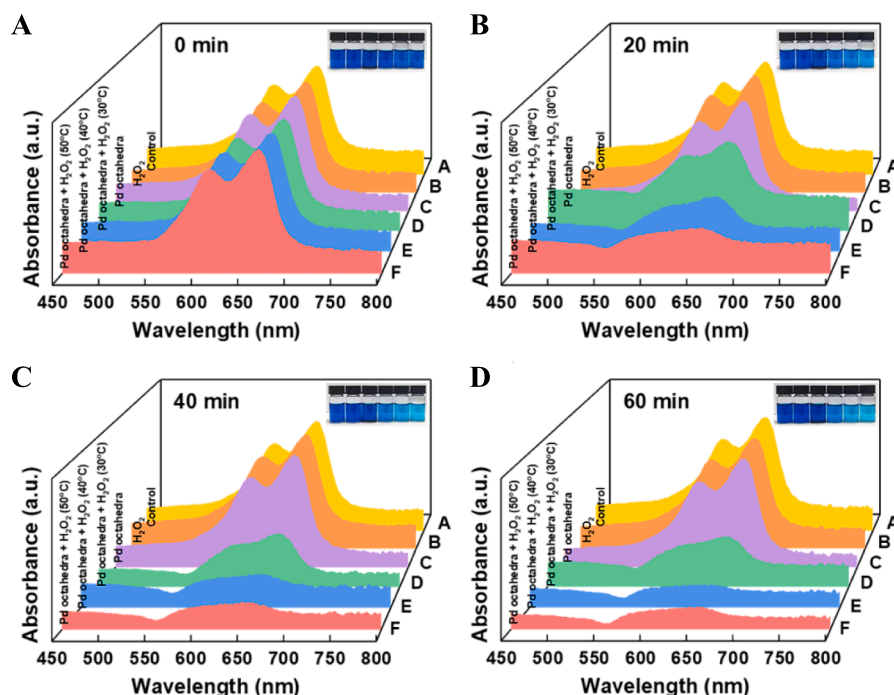


Fig. 5. UV-Vis absorption spectra of solutions under various catalytic systems at different periods such as (A) 0, (B) 20, (C) 40, and (D) 60 min.

the highest temperature exhibited the most efficient MB degradation. Moreover, the corresponding reaction rate constants rose with increasing temperature and the highest reaction rate constant (50 °C water bath group) was 0.0305 min⁻¹ (Fig. 4F).

Next, we used the degradation rate under 50 °C water bath group as a control and investigated the ability of Pd octahedra to remove MB from solution under 808 nm NIR laser irradiation (1.6 W cm⁻²). As illustrated in Fig. 6A, during the initial 40 min of degradation, the degradation efficiency of the 808 NIR laser group was inferior to that of the water bath heating group. This difference could be attributed to the time needed for Pd octahedra to reach the required temperature. Once reaching a stable peak temperature state, the degradation efficiency of MB rapidly accelerated, eventually surpassing that of the water bath group. The degradation rate of the laser group at 70 min was approximately 80 %. These results collectively underscore that Pd octahedra, serving as a stable photothermal adjuvant, can notably enhance the degradation efficiency of the Fenton reaction toward dye wastewater.

3.5. Influences of various factors on the MB degradation efficiency

To enhance the degradation efficiency of MB and identify the optimal conditions for the catalytic reaction, we examined the impacts of catalyst concentration, pH value, and dye concentration. By employing varying concentrations of Pd octahedra to degrade MB, as depicted in Fig. 6C, we observed that with an increase in catalyst dosage, the catalytic efficacy improved, resulting in a corresponding augmentation of the MB removal rate. This improvement can be ascribed to the heightened concentration of the catalyst, which provides additional adsorption sites and active sites for the catalytic reaction. Given that higher doses of Pd octahedra may escalate treatment expenses, we prefer utilizing lower concentrations of the catalyst. Fig. 6D illustrates that elevating the MB content in wastewater leads to a reduction in the removal rate. This decline stems from the limited availability of the catalyst, once the catalytic activity saturates, the reaction gradually decelerates, rendering it incapable of completely degrading the MB components in the system.

The pH level consistently plays a pivotal role in influencing Fenton

catalytic reaction. Thus, our investigation focused on assessing the impact of initial pH values on the Fenton degradation of MB. As depicted in Fig. 6B, within the photo-Fenton catalytic system, a pH of 5 demonstrated the most efficient catalytic degradation facilitated by Pd octahedra. Utilizing 125 μg mL⁻¹ of catalyst, complete removal of MB waste from the solution was achieved within 35 min. To summarize the sensitivity of the catalyst to pH, it exhibited heightened catalytic activity under acidic conditions while displaying diminished activity under alkaline conditions. This could be attributed to the fact that some of the Pd octahedra exist in the form of cations, which are prone to form Pd (OH)₂ precipitates under alkaline conditions, thus weakening the Fenton catalytic reaction.

3.6. Recyclability and stability of Pd octahedra

The recyclability and structural stability of catalysts are critical factors affecting their industrial application. Therefore, we evaluated the reusability of Pd octahedra catalysts by cycling experiments. As shown in Fig. 6E, the degradation efficiency of MB could still reach more than 90 % even after five cycles, indicating excellent reusability of the obtained Pd octahedra. In addition, as can be seen in Fig. 6F, the morphology of Pd octahedra has not changed significantly after reuse for five times, which further confirming the stability of Pd octahedra.

These results collectively demonstrate the outstanding stability and reusability of Pd-based catalysts. More importantly, compared to the recent catalytic systems reported in Table 1, Pd octahedra synthesised in this study exhibited the best degradation performance of MB.

3.7. Mechanism of Fenton catalytic reaction

We investigated the degradation mechanism of Pd octahedra. EPR spectroscopy analysis, utilizing DMPO as a spin trapping agent, was employed to visually track the generation and change of •OH. As depicted in Fig. 7A, no EPR signal was detected under H₂O₂-free condition. However, in the Pd octahedra/H₂O₂ system, a robust quartet signal with an intensity ratio of 1:2:2:1 was observed, indicating the Pd octahedra has the capability to activate H₂O₂ and generate •OH.

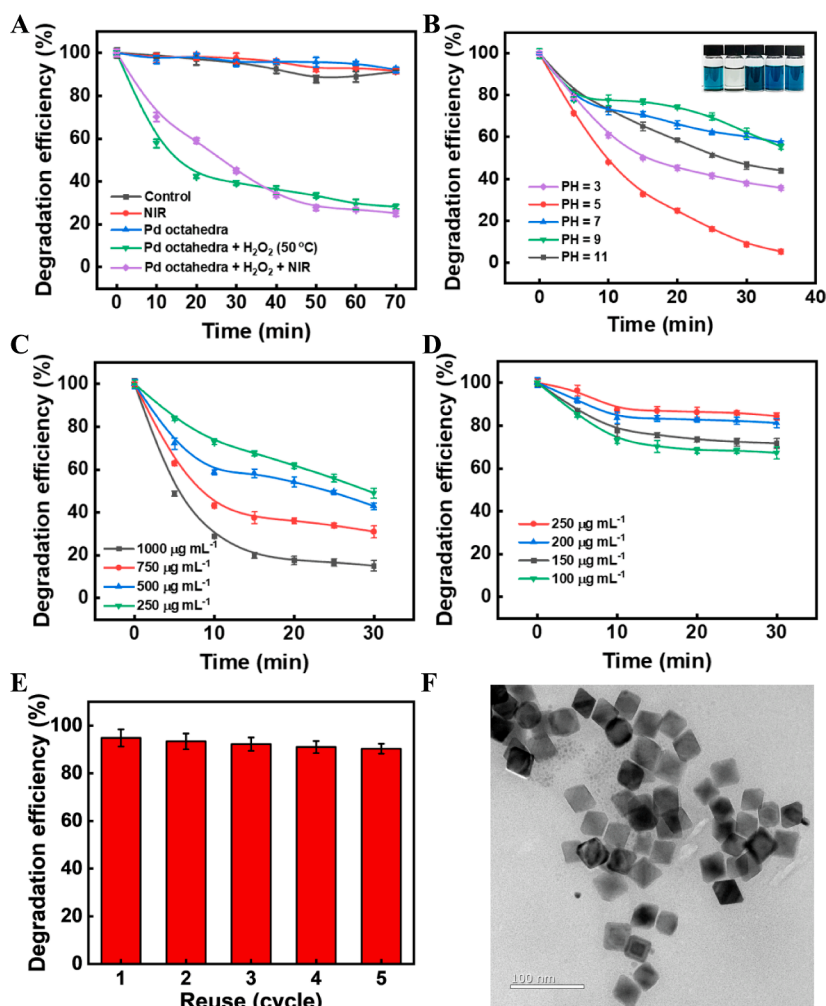


Fig. 6. Degradation efficiency curves of MB under varied (A) catalytic systems, (B) pH levels (Concentration of Pd octahedra: $125.0 \mu\text{g mL}^{-1}$, H_2O_2 : 3 %, MB: 50 mg/L), (C) Pd octahedra concentrations, and (D) MB concentrations. (E) MB degradation efficiency after five cycles. (F) TEM image of Pd octahedra after reuse for five times.

Table 1
Degradation efficiency between different Fenton catalytic system.

Catalyst	MB (g/L)	H_2O_2 (%)	Catalyst dosage (g L^{-1})	Efficiency (%)	Time (min)	Reference
Pd octahedra	0.05	3	0.125	94.8	35	This work
PdCuAu NAs	0.05	6	2	97	35	(Zhang et al., 2023)
$\text{NH}_2\text{-MIL-88B(Fe)}$	0.02	0.6	0.2	>99	50	(He et al., 2018)
$\text{Cu}_2\text{O@Sn}_2\text{O@PDA}$	0.05	5	0.5	>99	120	(Gao et al., 2023)

Furthermore, the $\bullet\text{OH}$ signal in the Fenton group under laser irradiation exhibited higher intensity, consistent with the results obtained from DFT calculations (Fig. 7B). This suggests that the photothermal performance of Pd octahedra can significantly augment the $\bullet\text{OH}$ generation ability from Fenton catalytic reaction.

TOC refers to the total amount of carbon contained in dissolved and suspended organic matter in water. Therefore, we used TOC as an evaluation index to calculate the TOC removal rate of different wastewater treatment groups according to Eq. (6), to measure the removal efficiency of MB. As shown in Fig. 7C, the Photo-Fenton catalytic group showed the highest TOC removal rate, additionally, the TOC removal rate of MB aqueous solution surpassed 50 % within 4 h.

$$\text{TOC removal rate (\%)} = \frac{\text{TOC}_0 - \text{TOC}_t}{\text{TOC}_0} * 100\% \quad (6)$$

In Eq. (6), TOC_0 represents the TOC content in the water before degradation, TOC_t represents the TOC content after degradation, and t (h) is the degradation time.

Based on the aforementioned experimental results, we propose a potential Fenton reaction mechanism illustrated in Fig. 7D, delineating the schematic diagram of $\bullet\text{OH}$ generation induced by Pd octahedra. Pd octahedra exist in both Pd^0 and Pd^{2+} form, upon NIR light irradiation, electron-hole pairs are generated on the surface of Pd octahedra. Pd^{2+} absorbs the electrons to form the transition state Pd^+ , which catalyzes the decomposition of nearby H_2O_2 , initiating the Fenton reaction while regenerating Pd^{2+} , thus enabling sustained self-catalytic cycling. Moreover, the photothermal effect of Pd octahedra significantly expedites the Fenton reaction. Throughout this process, a substantial quantity of $\bullet\text{OH}$ is continuously produced. Ultimately, the potent oxidative capacity of $\bullet\text{OH}$ decomposes MB into smaller molecules such as CO_2 and

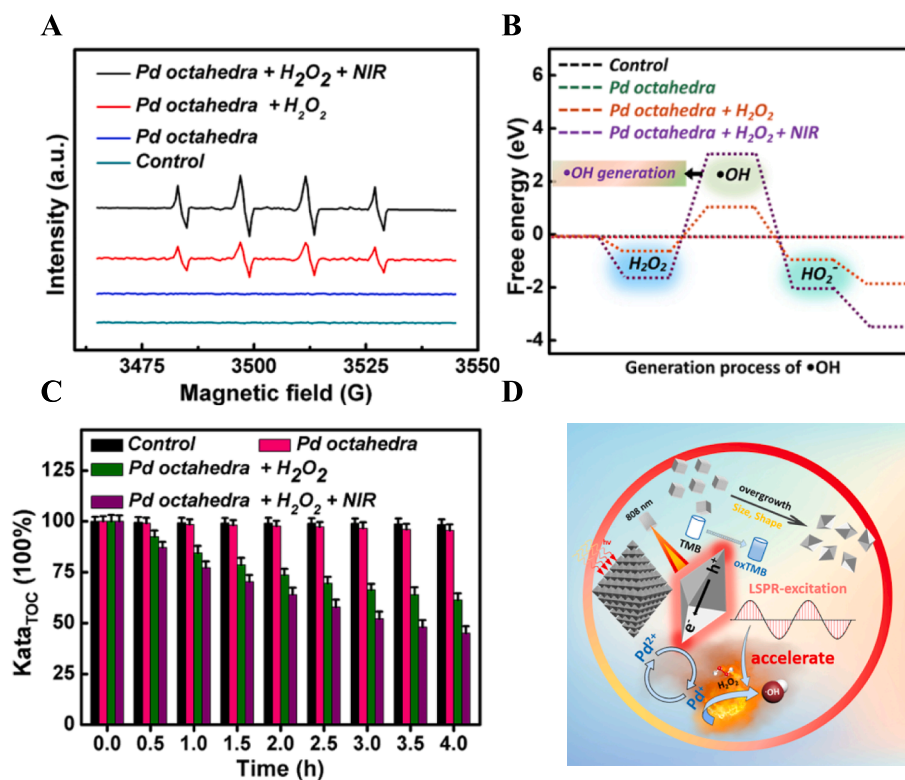
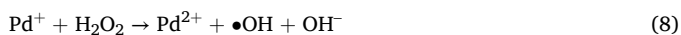


Fig. 7. (A) EPR spectra and (B) DFT calculation of $\bullet\text{OH}$ under different catalytic systems. (C) TOC content remaining in water across varying time intervals. (D) Schematic diagram illustrating the mechanism of $\bullet\text{OH}$ generation in the photo-Fenton catalytic system.

H_2O . The principal equations involved in this reaction are as follows:



3.8. Possible degradation pathways of MB

To further elucidate the Fenton oxidation pathway and degradation mechanism of MB facilitated by Pd octahedra, we performed GC–MS and IC analyses on MB solutions degraded for 30 and 60 min, and the intermediate products in the degradation of MB were analyzed to include organic compounds such as toluene, styrene, phenol, p-nitrophenol, 2,4,6-trimethylphenol, and 4-aminobenzenethiol, and anionic compounds such as Cl^- , NO_3^- , and SO_3^{2-} , as shown in Fig. 8A and 8B. By examining the interrelations among these intermediates, we proposed a conceivable degradation pathway for the Fenton catalytic oxidation of MB.

As delineated in Fig. 8C, upon dissolution of MB molecules in water, Cl^- are initially dissociated. Under the influence of active species like $\bullet\text{OH}$, involving processes such as electrophilic addition, electron transfer, and electron attack, the N- CH_3 bond undergoes cleavage, leading to the detachment of the chromophoric group ($-\text{CH}_3$), oxidation of the N-dimethylamino group to an amino group ($-\text{NH}_2$), and the demethylation can result in significant decolorization of the MB solution. Concurrently, the C-S single bond on the central heterocycle of MB is cleaved, with the S atom possibly oxidized to SO_4^{2-} . As the reaction proceeds, the amino group is either eliminated to form NH_4^+ or oxidized to NO_3^- . Subsequently, under the influence of active species, the generated intermediate products undergo benzene ring opening, bond cleavage, and addition reactions, ultimately undergoing oxidative decomposition into

CO_2 , H_2O , and inorganic ions. All oxidation reaction steps are facilitated by $\bullet\text{OH}$ generated by the Fenton reaction.

3.9. Cellular toxicity assessment

MTT assay is commonly used to assess cell viability and growth, the detection principle is that the succinate dehydrogenase in the mitochondria of living cells can reduce exogenous MTT to formazan, while dead cells lack this function. The luciferase assay utilizes the “luciferase-luciferin system” to rapidly detect the ATP levels in living cells, thus reflecting cell quantity. Therefore, we employed the MTT assay and the luciferase assay to evaluate the biocompatibility and cytotoxicity of Pd octahedra. After Pd octahedra and cells were co-incubated in 96-well plates for 24 h, MTT solution and ATP reaction solution were added respectively. The absorption value at 490 nm was measured by using enzyme-linked immunometric meter, and the fluorescence intensity was detected by using an ATP fluorescence detector, which ultimately led to the cell number, viability, and cellular energy metabolism after incubation. Results depicted in Fig. 8D and 8E demonstrated that even at elevated concentrations of Pd octahedra, cellular metabolic activity remained above 95%. Hence, the Pd octahedra catalytic system established in this study was deemed non-toxic to cells and compatible with biological systems, posing no secondary pollution to the water body. It stands as a safe and efficient solution for addressing dye treatment in wastewater, promoting sustainability and eco-friendliness.

4. Conclusion

In summary, we successfully synthesized Pd octahedra with high aspect ratio and tip-shaped nanostructure by controlling the shape and size of Pd cubes. Harnessing the surface plasmon resonance effect of Pd octahedra, we attained excellent photothermal conversion efficiency in the NIR region. The inherent peroxidase-like activity of Pd octahedra qualifies it as Fenton-like reagents, facilitating the catalytic degradation

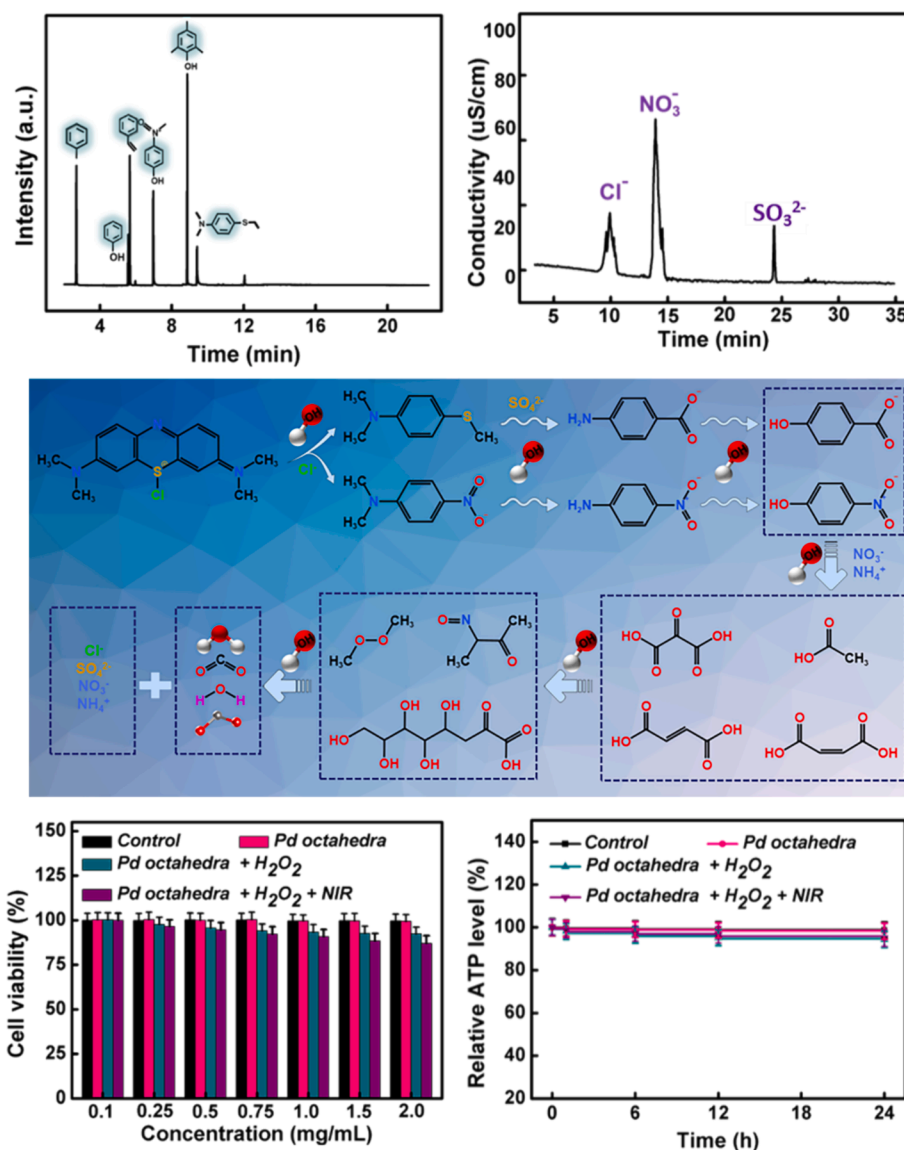


Fig. 8. (A) GC-MS and (B) IC analyses on MB solutions during degradation. (C) Potential decomposition processes of MB. (D) Cell viability and (E) relative ATP level after co-culturing with Pd octahedra.

of MB in wastewater. The integration of catalytic and photothermal centers within Pd octahedra enhances local temperature during reaction, thereby expediting catalysis and optimizing reaction kinetics. In conclusion, our Pd-based Fenton catalytic system is biocompatible and proficiently degrades and mineralizes MB in wastewater.

CRedit authorship contribution statement

Heying Li: Writing – original draft, Data curation. **Ding Luo:** Software, Formal analysis, Data curation. **Pengshan Guo:** Methodology, Formal analysis. **Shegan Gao:** Writing – review & editing, Validation. **Manping Lin:** Software. **Hongbo Sun:** Supervision, Methodology. **Jianping Wang:** Writing – review & editing, Validation. **Dongmei Yu:** Methodology, Data curation. **Shaowen Cheng:** Writing – review & editing. **Jinghua Li:** Writing – review & editing, Project administration.

Declaration of competing interest

The authors declare that they have no known competing financial interests or personal relationships that could have appeared to influence the work reported in this paper.

Acknowledgment

This work was supported by National Natural Science Foundation of China (No. 32260237, 11962005). Natural Science Foundation of Hainan Province (No. 823MS045, 2019RC375). The study was supported by Qinghai Provincial Key Laboratory of Geology and Environment of Salt Lakes (No. The Science and Technology Plan Project of Qinghai Province Incentive Fund 2022-2024). Hainan Province Higher Education Teaching Reform Research Project (No. Hnjg2024ZD-36 and Hnjg2024-80).

References

- Ali, S., Chen, X., Ahmad, S., Almeahmadi, M., Alsaiari, A.A., Allahyani, M., Gul, Z., Ullah, A., Hussain, H., Li, L., Chen, X., 2023. Morphology-controllable bimetallic gold nanostructures for mercury detection: Recent developments, challenges and prospects. *Arabian J Chem* 16, 104997.
- Awiaz, G., Lin, J., Wu, A., 2023. Recent advances of Au@Ag core-shell SERS-based biosensors. *Exploration (beijing)* 3, 20220072.
- Bi, G., Ding, R., Song, J., Luo, M., Zhang, H., Liu, M., Huang, D., Mu, Y., 2024. Discriminating the active ru species towards the selective generation of singlet oxygen from peroxydisulfate: Nanoparticles surpass single-atom catalysts. *Angew Chem Int Ed Engl* 63, e202401551.

- Chen, T., Chu, Q., Li, M., Han, G., Li, X., 2021. Fe₃O₄@Pt nanoparticles to enable combinational electrodynamic/chemodynamic therapy. *J Nanobiotechnology* 19, 206.
- Chow, T.H., Li, N., Bai, X., Zhuo, X., Shao, L., Wang, J., 2019. Gold nanobipyramids: An emerging and versatile type of plasmonic nanoparticles. *Acc Chem Res* 52, 2136–2146.
- Gao, J., Cheng, S., Zhou, P., Zhang, J., Li, H., Zhang, Y., Lin, M., Gu, S., Li, J., 2023. Fenton-driven photothermal enhanced degradation of methylene blue by using Cu₂O@SnO₂@PDA cubic heterostructured catalyst. *Mater Lett* 334, 133724.
- He, J., Zhang, Y., Zhang, X., Huang, Y., 2018. Highly efficient Fenton and enzyme-mimetic activities of NH₂-ML-88B(Fe) metal organic framework for methylene blue degradation. *Sci Rep* 8, 5159.
- Jana, D., Zhao, Y., 2022. Strategies for enhancing cancer chemodynamic therapy performance. *Exploration (beijing)* 2, 20210238.
- Kesharwani, P., Ma, R., Sang, L., Fatima, M., Sheikh, A., Abourehab, M.A.S., Gupta, N., Chen, Z.S., Zhou, Y., 2023. Gold nanoparticles and gold nanorods in the landscape of cancer therapy. *Mol Cancer* 22, 98.
- Kim, S., Wang, R., Dhandapani, S., Kang, K., Cho, I.-H., Kim, Y.-J., 2024. Novel modified probiotic gold nanoparticles loaded with ginsenoside CK exerts an anti-inflammation effect via NF-κB/MAPK signaling pathways. *Arabian J Chem* 17, 105650.
- Li, C., Ye, J., Yang, X., Liu, S., Zhang, Z., Wang, J., Zhang, K., Xu, J., Fu, Y., Yang, P., 2022. Fe/Mn bimetal-doped ZIF-8-coated luminescent nanoparticles with up/downconversion dual-mode emission for tumor self-enhanced NIR-II imaging and catalytic therapy. *ACS Nano* 16, 18143–18156.
- Lian, Z., Gao, F., Xiao, H., Luo, D., Li, M., Fang, D., Yang, Y., Zi, J., Li, H., 2024. Photo-self-fenton reaction mediated by atomically dispersed Ag-Co photocatalysts toward efficient degradation of organic pollutants. *Angew Chem Int Ed Engl* 63, e202318927.
- Liao, Q., Zhu, K., Hao, X., Wu, C., Li, J., Cheng, H., Yan, J., Jiang, L., Qu, L., 2024. Bio-inspired ultrathin perfect absorber for high-performance photothermal conversion. *Adv Mater* e2313366.
- Liu, H.Z., Shu, X.X., Huang, M., Wu, B.B., Chen, J.J., Wang, X.S., Li, H.L., Yu, H.Q., 2024. Tailoring d-band center of high-valent metal-oxo species for pollutant removal via complete polymerization. *Nat Commun* 15, 2327.
- Liu, Z., Su, R., Xu, F., Xu, X., Gao, B., Li, Q., 2024. The unique Fe₃Mo₃N structure bestowed efficient fenton-like performance of the iron-based catalysts: the double enhancement of radicals and nonradicals. *Adv Mater* e2311869.
- Lu, N., Liu, F., 2024. Temporarily confined catalytic membranes for advanced water remediation. *Adv Mater* e2311419.
- Lushaj, E., Bordin, M., Akbar, K., Liccardo, L., Barroso-Martín, I., Rodríguez-Castellón, E., Vomiero, A., Moretti, E., Polo, F., 2024. Highly efficient solar-light-driven photodegradation of metronidazole by nickel hexacyanoferrate nanocubes showing enhanced catalytic performances. *Small Methods* e2301541.
- Meng, W., Sun, S., Xie, D., Dai, S., Shao, W., Zhang, Q., Qin, C., Liang, G., Li, X., 2024. Engineering defective Co₃O₄ containing both metal doping and vacancy in octahedral cobalt site as high performance catalyst for methane oxidation. *Mol Catal* 553, 113768.
- Palani, S., Kenison, J.P., Sabuncu, S., Huang, T., Civitci, F., Esener, S., Nan, X., 2023. Multispectral localized surface plasmon resonance (msLSPR) reveals and overcomes spectral and sensing heterogeneities of single gold nanoparticles. *ACS Nano* 17, 2266–2278.
- Ren, W., Yan, Y., Zeng, L., Shi, Z., Gong, A., Schaaf, P., Wang, D., Zhao, J., Zou, B., Yu, H., Chen, G., Brown, E.M.B., Wu, A., 2015. A near infrared light triggered hydrogenated black TiO₂ for cancer photothermal therapy. *Adv Healthc Mater* 4, 1526–1536.
- Schuknecht, F., Kolataj, K., Steinberger, M., Liedl, T., Lohmueller, T., 2023. Accessible hotspots for single-protein SERS in DNA-origami assembled gold nanorod dimers with tip-to-tip alignment. *Nat Commun* 14, 7192.
- Seo, S.H., Kim, B.M., Joe, A., Han, H.W., Chen, X., Cheng, Z., Jang, E.S., 2014. NIR-light-induced surface-enhanced Raman scattering for detection and photothermal/photodynamic therapy of cancer cells using methylene blue-embedded gold nanorod@SiO₂ nanocomposites. *Biomaterials* 35, 3309–3318.
- Sibug-Torres, S.M., Grys, D.B., Kang, G., Niihori, M., Wyatt, E., Spiesshofer, N., Ruane, A., de Nijs, B., Baumberg, J.J., 2024. In situ electrochemical regeneration of nanogap hotspots for continuously reusable ultrathin SERS sensors. *Nat Commun* 15, 2022.
- Skillin, N.P., Bauman, G.E., Kirkpatrick, B.E., McCracken, J.M., Park, K., Vaia, R.A., Anseth, K.S., White, T.J., 2024. Photothermal actuation of thick 3D-printed liquid crystalline elastomer nanocomposites. *Adv Mater* e2313745.
- Tian, M., Liu, Y., Zhang, S., Yu, C., Ostrikov, K.K., Zhang, Z., 2024. Overcoming the permeability-selectivity challenge in water purification using two-dimensional cobalt-functionalized vermiculite membrane. *Nat Commun* 15, 391.
- Tian, L., Tang, Z.J., Hao, L.Y., Dai, T., Zou, J.P., Liu, Z.Q., 2024. Efficient homolytic cleavage of H₂O₂ on hydroxyl-enriched spinel CuFe₂O₄ with dual lewis acid sites. *Angew Chem Int Ed Engl* 63, e202401434.
- Wang, L.C., Chiou, P.Y., Hsu, Y.P., Lee, C.L., Hung, C.H., Wu, Y.H., Wang, W.J., Hsieh, G. L., Chen, Y.C., Chang, L.C., Su, W.P., Manoharan, D., Liao, M.C., Thangudu, S., Li, W. P., Su, C.H., Tian, H.K., Yeh, C.S., 2023. Prussian blue analog with separated active sites to catalyze water driven enhanced catalytic treatments. *Nat Commun* 14, 4709.
- Wu, X.L., Liu, S., Li, Y., Yan, M., Lin, H., Chen, J., Liu, S., Wang, S., Duan, X., 2023. Directional and ultrafast charge transfer in oxygen-vacancy-rich ZnO@single-atom cobalt core-shell junction for photo-fenton-like reaction. *Angew Chem Int Ed Engl* 62, e202305639.
- Yan, Q., Lian, C., Huang, K., Liang, L., Yu, H., Yin, P., Zhang, J., Xing, M., 2021. Constructing an acidic microenvironment by MoS₂ in heterogeneous fenton reaction for pollutant control. *Angew Chem Int Ed Engl* 60, 17155–17163.
- Yan, H., Peng, Y., Huang, Y., Shen, M., Wei, X., Zou, W., Tong, Q., Zhou, N., Xu, J., Zhang, Y., Ye, Y.X., Ouyang, G., 2024. Enhancing photosynthesis efficiency of hydrogen peroxide by modulating side chains to facilitate water oxidation at low-energy barrier sites. *Adv Mater* e2311535.
- Yang, Y., Jia, H., Hu, N., Zhao, M., Li, J., Ni, W., Zhang, C.Y., 2024. Construction of gold/rhodium freestanding superstructures as antenna-reactor photocatalysts for plasmon-driven nitrogen fixation. *J Am Chem Soc* 146, 7734–7742.
- Yang, J., Yang, Z., Li, J., Gang, H., Mei, D., Yin, D., Deng, R., Zhu, Y., Li, X., Wang, N., Osman, S.M., Yamauchi, Y., 2024. Engineering a hollow bowl-like porous carbon-confined Ru-MgO hetero-structured nanopair as a high-performance catalyst for ammonia borane hydrolysis. *Mater Horiz* 11, 2032–2040.
- Yu, Z., Jin, X., Guo, Y., Liu, Q., Xiang, W., Zhou, S., Wang, J., Yang, D., Wu, H.B., Wang, J., 2024. Decoupled oxidation process enabled by atomically dispersed copper electrodes for in-situ chemical water treatment. *Nat Commun* 15, 1186.
- Yu, D., Xu, L., Fu, K., Liu, X., Wang, S., Wu, M., Lu, W., Lv, C., Luo, J., 2024. Electronic structure modulation of iron sites with fluorine coordination enables ultra-effective H₂O₂ activation. *Nat Commun* 15, 2241.
- Zhang, W., Cai, K., Sun, Z., Xiang, Q., Yuan, L., Fu, M., Liu, X., Foda, M.F.F., Ye, Z., Huang, J., Liu, H., Han, H., Liang, H., Dong, H., Zhang, X., 2023. Elevating second near-infrared photothermal conversion efficiency of hollow gold nanorod for a precise theranostic of orthotopic bladder cancer. *ACS Nano* 17, 18932–18941.
- Zhang, L., Røling, L.T., Wang, X., Vara, M., Chi, M., Liu, J., Choi, S.I., Park, J., Herron, J. A., Xie, Z., Mavrikakis, M., Xia, Y., 2015. Nanocatalysts platinum-based nanocages with subnanometer-thick walls and well-defined, controllable facets. *Science* 349, 412–416.
- Zhang, L., Chen, Y., Zheng, J., Lewis, G.R., Xia, X., Ringe, E., Zhang, W., Wang, J., 2023. Chiral gold nanorods with five-fold rotational symmetry and orientation-dependent chiroptical properties of their monomers and dimers. *Angew Chem Int Ed Engl* 62, e202312615.
- Zhang, J., Lei, K., Cheng, J., Luo, L., Xi, L., Li, J., 2023. Sea urchin-like PdCuAu nanoclusters mediated photothermal enhanced Fenton catalysis for degradation of dye pollutants. *J Alloys Compd* 958, 170494.
- Zhang, D., Li, Y., Wang, P., Qu, J., Li, Y., Zhan, S., 2023. Dynamic active-site induced by host-guest interactions boost the Fenton-like reaction for organic wastewater treatment. *Nat Commun* 14, 3538.
- Zhang, X., Tang, J., Wang, L., Wang, C., Chen, L., Chen, X., Qian, J., Pan, B., 2024. Nanocage-triggered oligomerization pathway for efficient removal of phenolic pollutants via a fenton-like reaction. *Nat Commun* 15, 917.
- Zhao, X., Tang, H., Jiang, X., 2022. Deploying gold nanomaterials in combating multi-drug-resistant bacteria. *ACS Nano* 16, 10066–10087.
- Zhao, X., Chen, Y., Niu, R., Tang, Y., Chen, Y., Su, H., Yang, Z., Jing, X., Guan, H., Gao, R., Meng, L., 2024. NIR plasmonic nanozymes: Synergistic enhancement mechanism and multi-modal anti-infection applications of MXene/MOFs. *Adv Mater* 36, e2307839.
- Zhu Y., Zhao R., Feng L., Wang W., Xie Y., Ding H., Liu B., Dong S., Yang P., Lin J., Defect-Engineered Tin Disulfide Nanocarriers as "Precision-Guided Projectile" for Intensive Synergistic Therapy, *Small Methods* (2024) e2400125.